

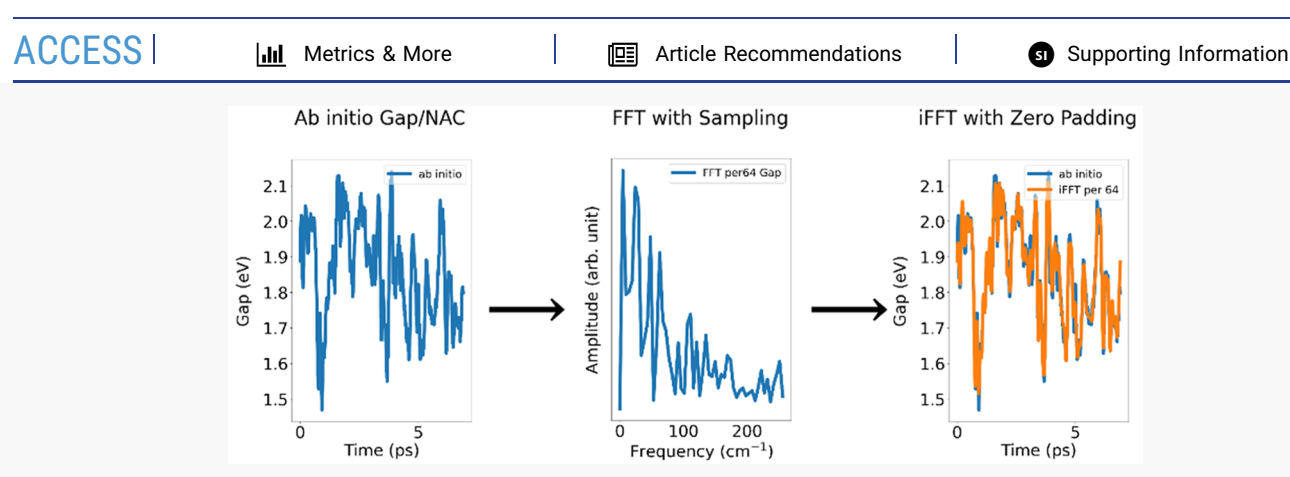
pubs.acs.org/JPCL Letter

# Interpolating Nonadiabatic Molecular Dynamics Hamiltonian with Inverse Fast Fourier Transform

Bipeng Wang, Weibin Chu, and Oleg V. Prezhdo\*







ABSTRACT: Nonadiabatic (NA) molecular dynamics (MD) allows one to investigate far-from-equilibrium processes in nanoscale and molecular materials at the atomistic level and in the time domain, mimicking time-resolved spectroscopic experiments. Ab initio NAMD is limited to about 100 atoms and a few picoseconds, due to computational cost of excitation energies and NA couplings. We develop a straightforward methodology that can extend ab initio quality NAMD to nanoseconds and thousands of atoms. The ab initio NAMD Hamiltonian is sampled and interpolated along a trajectory using a Fourier transform, and then, it is used to perform NAMD with known algorithms. The methodology relies on the classical path approximation, which holds for many materials and processes. To achieve a complete ab initio quality description, the trajectory can be obtained using an ab initio trained machine learning force field. The method is demonstrated with charge carrier trapping and relaxation in hybrid organic—inorganic and all-inorganic metal halide perovskites that exhibit complex dynamics and are actively studied for optoelectronic applications.

onadiabatic (NA) molecular dynamics (MD) is a powerful tool for modeling excited-state dynamics in molecules and condense matter systems. NAMD simulations emulate time-resolved spectroscopy experiments and present useful insights into naturally occurring non-equilibrium phenomena at the atomistic level. 1–8 In order to perform an NAMD simulation, knowledge of energies of different electronic states and NA couplings (NACs) between the states is required. The energies and NAC depend on nuclear coordinates. In small systems, the nuclear dependence of the electronic properties can be mapped in advance for the whole range of nuclear coordinates. In larger systems, the accessible space of nuclear coordinates is too large, and "on-the-fly" ab initio electronic structure calculations are performed along NAMD trajectories. Condensed phase systems contain large numbers of electrons, and frequently, excitation of one or a few electrons has a minor influence on nuclear geometries, as compared to thermal nuclear fluctuations. Alternatively, relaxation through dense manifolds of electronic states, present in condensed phase systems, occurs rapidly and the geometry does not have time to respond to the excitation. In such cases, the classical path approximation (CPA) can be employed, 9,10

under which MD trajectories are generated for the ground<sup>11–13</sup> or low-energy excited electronic states,<sup>14–16</sup> and these trajectories are used to drive the non-equilibrium electronic evolution. The CPA reduces the computational cost of ab initio calculations by orders of magnitude, because multiple NAMD trajectories are replaced with a single trajectory, expensive excited-state force calculations are replaced with ground-state calculations, and the NA Hamiltonian is updated on a nuclear rather than electronic time step. Still, even under the CPA, the ab initio calculations required to perform NAMD simulations are expensive if systems are large, and further advances are required in order to perform atomistic modeling of modern complex materials and processes.

Received: November 27, 2021 Accepted: December 29, 2021 Published: January 3, 2022





Structural motifs of condensed matter systems are used to generate descriptors and replace conventional ab initio calculations with more computationally efficient machine learning (ML) models, which include artificial neural networks (NNs), convolutional NNs, kernel ridge regression (KRR), and so on. Development of ML force fields (FF) based on ab initio data has allowed scientists to greatly extend the range of ab initio quality MD simulations in both system size and time scale. 17-19 A variety of structural fingerprint methodologies have been proposed, such as extended-connectivity fingerprints,<sup>20</sup> smooth overlap of atomic positions,<sup>21</sup> and Behler-Parrinello symmetry functions.<sup>22</sup> These efforts have successfully mapped nuclear geometries and atomic information onto various chemical properties, finding nonlinear patterns between the properties and digital fingerprints. 23-29 However, the ML methods require significant amounts of ab initio data to validate hyperparameters, generating high computational cost. Application of ML to NAMD carries additional cost, since ab initio calculations required to obtain excitation energies and NACs are more expensive than ground-state calculations. Moreover, excited-state energies and NACs exhibit more complex dependence on nuclear geometries than ground-state energies, and the number of NACs scales quadratically with the number of electronic states. All of these factors make application of ML to NAMD computationally expensive and complicated compared, for example, to development of MLFFs. Fortunately, the CPA allows for an alternative strategy,<sup>30</sup> in which the NAMD Hamiltonian is interpolated along a precomputed trajectory that can be obtained with a MLFF.31 Because only the scalar form of the NAC is needed under the CPA, one can employ a simpler set of descriptors for NAC interpolation compared to those used to generate a

In this letter, we demonstrate that an efficient interpolation of the NAMD Hamiltonian generated under the CPA can be achieved by inverse fast Fourier transform (iFFT). This strategy is notably simpler than the use of NNs<sup>30</sup> and KRR,<sup>32</sup> while at the same time the needed training data set is even smaller. The iFFT method requires much less time and effort than training a ML model, while it gives reliable NAMD results that converge to the ab initio calculations. We demonstrate the method with nonradiative charge relaxation in two metal halide perovskites (MHPs), one of which has a defect that creates a mid-gap trap state, while the other contains high-frequency vibrations that potentially can require frequent sampling. A small fraction (1.56%) of excitation energies and NAC sampled along the MD trajectory is sufficient to obtain highquality results in all cases, reducing the NAMD computational cost by nearly 2 orders of magnitude.

MHPs have gained significant attention because of low manufacturing cost and excellent optoelectronic properties, such as strong light absorption, tunable band gap, small exciton binding energy, and long charge carrier lifetime.<sup>33–36</sup> The power conversion efficiency of perovskite solar cells has exceeded 25.2%,<sup>37</sup> while this number was only 14.2% in 2013.<sup>38</sup> Relatively soft materials containing both inorganic and organic components, MHPs exhibit complicated nuclear motions occurring over a large range of time scales and creating challenges for NAMD simulations.

We apply the iFFT-NAMD method to the organic—inorganic CH<sub>3</sub>NH<sub>2</sub>PbI<sub>3</sub> (MAPbI<sub>3</sub>) perovskite, the all-inorganic CsPbI<sub>3</sub> perovskite, and the all-inorganic CsPbI<sub>3</sub> perovskite in which a cesium atom is replaced by an iodine atom, Figure 1.

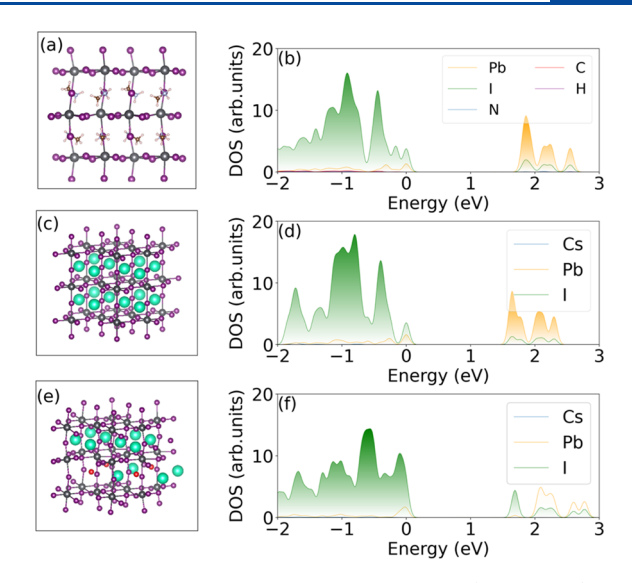


Figure 1. Optimized ground-state geometries (left panels) and projected DOS (right panels) for (a, b) pristine MAPbI<sub>3</sub>, (c, d) pristine CsPbI<sub>3</sub>, and (e, f) defective CsPbI<sub>3</sub> with Cs atom replaced by I (marked as red). The VBM energy is set to zero. In all three perovskite systems, the VBM and CBM are primarily contributed by iodine and lead/iodine, respectively. The defect creates a mid-gap electron trap state.

In both pristine MAPbI<sub>3</sub> and CsPbI<sub>3</sub> systems, a direct band gap separates the valence band maximum (VBM) and the conduction band minimum (CBM). The 0 K gaps are 1.64 and 1.43 eV, respectively. The replacement of cesium with iodine introduces an empty electron trap state 0.17 eV below the CBM. The projected density of states (DOS) obtained for the optimized structures are shown in Figure 1. In all three cases, the VBM is mainly supported by I atoms, while the CBM is primarily supported by Pb atoms. The trap state in the defective CsPbI<sub>3</sub> perovskite is localized on the I atom that has replaced a Cs atom, as well as on other iodine atoms around the defect, presenting a favorable chemical environment for fast trapping of free electrons.

$$\begin{split} d_{ij} &= -i\hbar \varphi_{j}(r, R(t)) |\nabla_{R}| \varphi_{i}(r, R(t)) \frac{\mathrm{d}R}{\mathrm{d}t} \\ &= -i\hbar \frac{\varphi_{j}(r, R(t)) |\nabla_{R} \varphi_{i}(r, R(t))|}{E_{i} - E_{i}} \frac{\mathrm{d}R}{\mathrm{d}t} \\ &= -i\hbar \varphi_{j}(\mathbf{r}, \mathbf{R}(t)) \left| \frac{\partial}{\partial t} \right| \varphi_{i}(\mathbf{r}, \mathbf{R}(t)) \\ &\approx -\frac{i\hbar}{2\Delta t} \{ \varphi_{j}(\mathbf{r}, \mathbf{R}(t)) |\varphi_{i}(\mathbf{r}, \mathbf{R}(t + \Delta t)) \\ &- \varphi_{j}(\mathbf{r}, \mathbf{R}(t + \Delta t)) |\varphi_{i}(\mathbf{r}, \mathbf{R}(t)) \} \end{split}$$

All ab initio calculations are performed using the VASP program<sup>39</sup> and the PBE density functional.<sup>40</sup> The structures are relaxed at 0 K and are heated to 300 K, reaching thermal equilibrium. After that, 6912 fs MD trajectories with 1 fs time step are obtained in the microcanonical ensemble. The NAC can be calculated analytically or numerically via infinitesimal increments in positions or time, eq 1. In the current calculation we compute the couplings numerically by considering overlap of wave functions at sequential MD time steps, as done

Table 1. Average Energy Gap, Average Absolute NAC, Root-Mean-Square (RMS) NAC, Pure-Dephasing Time, and Charge Recombination Time Obtained from the Ab Initio and iFFT Hamiltonians for the Pristine MAPbI<sub>3</sub> and CsPbI<sub>3</sub> Systems

	$MAPbI_3$				$CsPbI_3$			
	ab initio	iFFT per64	iFFT per128	iFFT per256	ab initio	iFFT per64	iFFT per128	iFFT per256
gap (eV)	1.85	1.85	1.85	1.86	1.89	1.89	1.89	1.89
Abs NAC (meV)	0.22	0.22	0.22	0.27	0.45	0.45	0.42	0.36
RMS NAC (meV)	0.33	0.32	0.29	0.33	0.54	0.54	0.51	0.43
pure-dephasing time (fs)	4.75	4.74	4.46	4.22	8.48	8.45	8.71	8.25
recombination time (ns)	97.21	98.23	114.71	80.56	89.20	90.13	96.99	182.07

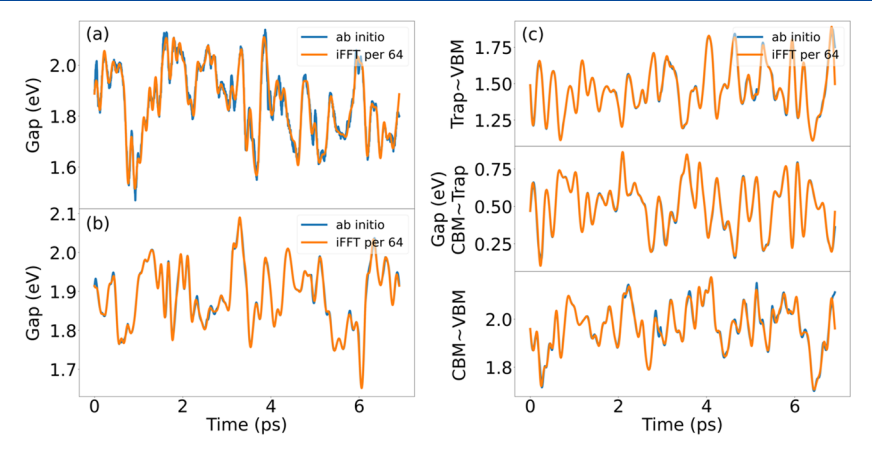


Figure 2. Energy gaps of (a) pristine MAPbI<sub>3</sub>, (b) pristine CsPbI<sub>3</sub>, and (c) defective CsPbI<sub>3</sub> predicted using the iFFT method. The data used to predict the entire trajectories are selected evenly every 64 points (1.56%, 108 points in total) from the ab initio data.

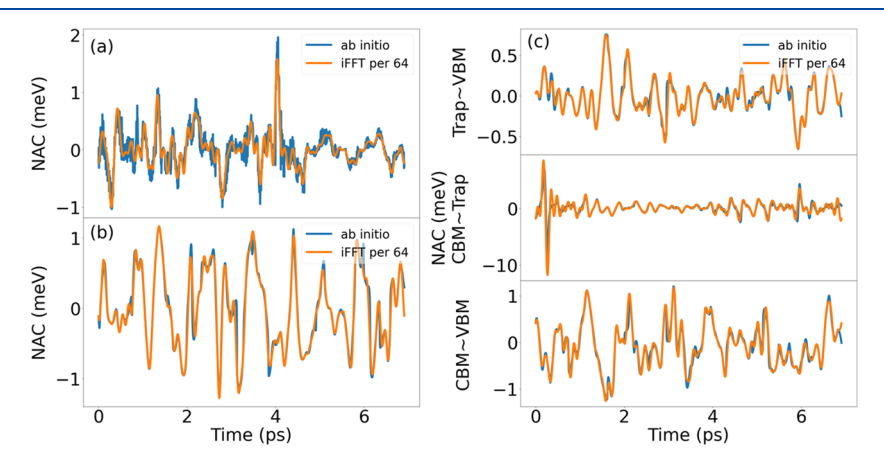
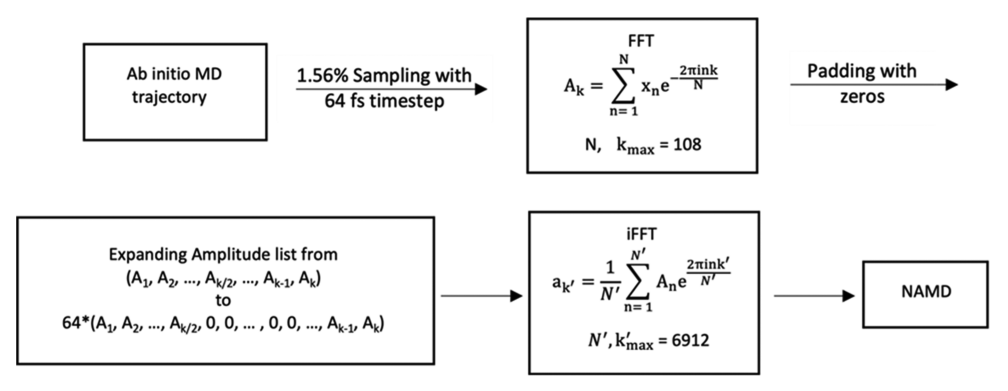


Figure 3. NACs of (a) pristine MAPbI<sub>3</sub>, (b) pristine CsPbI<sub>3</sub>, and (c) defective CsPbI<sub>3</sub> predicted using the iFFT method. The data used to predict the entire trajectories are selected evenly every 64 points (1.56%, 108 points in total) from the ab initio data.

#### Chart 1. Scheme of the iFFT-NAMD method



customarily under the CPA. Selection of the sampled ab initio data set is important for the iFFT method. On the one hand, FFT is best performed on data points that are equally spaced along the trajectory and are separated by  $2^n$  time steps. On the other hand, the sampling frequency needs to be sufficiently high in order to represent important oscillations in the NAMD Hamiltonian parameters. Largest amplitude peaks in a frequency analysis of excitation energy and NAC happen in the low-frequency domain, indicating that sparse data sampling may be sufficient. However, too sparse a sampling can result in loss of chemical information. In general, a short ab initio trajectory is needed for a particular system in order to determine how frequently the energy gaps and NAC have to be sampled. To balance the computational cost and chemical information, we sample 1.56% of the ab initio data equally spaced along the MD trajectory: 108 points spaced every 64 fs are used. The remaining 98.44% of the data, or 6804 data points, are employed for testing. An advantage of the iFFT method compared to NNs is that no extra data are needed for validation, while a NN relies heavily on validation for parameter tuning, since it is a parametrized model. In order to test the performance of the iFFT method in more stringent cases, subsets with 0.78% and 0.39% data are tested as well. The results are summarized in Table 1 and Supporting Information Table S1. The time-domain comparison of the ab initio and iFFT Hamiltonians can be found in Figures 2, 3 and S1-S4.

The methodology was implemented using the Python language. Chart 1 shows the scheme of the iFFT-NAMD method. In the process, the frequency information on the 1.56% excitation energies and NACs of the three MPHs are computed by the FFT function in the SciPy package. 41 After performing the FFT of the sampled data, the positions of the peaks are maintained, while their amplitudes are expanded 64 times to account for the fact that the amplitude is proportional to the number of data points and that every 64th point of the original data has been sampled. To interpolate the excitation energies and NACs, frequency information with the same length as that from the complete data set is created on the basis of the sampled data. "Zero padding", which adds additional zeros to the sampled amplitude, is used. By adding extra zeros, in this case 6804 zeros, the short, sampled frequency range is extended to the range corresponding to the FT of the full MD trajectory, which has 6912 points. Then, the iFFT function is applied on the zero-padded amplitude list, returning the interpolated excitation energy and NAC values in the time domain. These values are used to perform NAMD simulations and to compare with the fully ab initio results. The NAMD simulations are performed using decoherence induced surface hopping (DISH), <sup>42</sup> as implemented in the Pyxaid software. <sup>9,10</sup>

Electronic excitation energies for pristine MAPbI<sub>3</sub>, pristine CsPbI<sub>3</sub>, and defective CsPbI<sub>3</sub>, calculated by the ab initio and iFFT methods are shown in Figure 2. Since defective CsPbI<sub>3</sub> contains a mid-gap trap state, three energy gaps are shown, including VBM—trap, CBM—trap, and CBM—VBM, Figure 1c. The iFFT predictions have an excellent agreement with the ab initio values, especially in the two CsPbI<sub>3</sub> systems, Figure 1b,c. With only 1.56% of data sampling, all fluctuations in the excitation energies are reproduced very well and only very few peaks are slightly underestimated. In comparison, some fluctuations in the energy gap of pristine organic—inorganic MAPbI<sub>3</sub> are underestimated or missed by the iFFT method. That is expected because the organic MA species contains

many high-frequency modes that cannot be represented by the sampling with the 64 fs period. The fastest frequencies arise from C—H and N—H vibrations with the period on the order of 10 fs. Although electrons and holes in MHPs are supported by the inorganic lattice and MA, Cs, and other A-site cations do not contribute to the electronic wave functions near the fundamental band gap, these A-site species can have an indirect influence on the electronic properties, as established for instance, by the unsupervised ML analyses. <sup>29,43</sup> Even with such sparse data sampling, the iFFT method gives good predictions of the energy gaps in these complex systems, compared to the ab initio calculations. Reducing the sampling frequency further created deviations; however, the global behavior is still reproduced, Figures S1 and S2.

The mean squared errors for the 1.56% sampling are 5  $\times$   $10^{-4}$  and 3  $\times$   $10^{-5}$  eV for the VBM–CBM band gaps in the pristine MAPbI<sub>3</sub> and CsPbI<sub>3</sub> systems, respectively. The errors are 2  $\times$   $10^{-4}$ , 1  $\times$   $10^{-4}$ , and 1  $\times$   $10^{-4}$  eV for the trap–VBM, CBM–trap, and CBM–VBM gaps in defective CsPbI<sub>3</sub>. The errors are very small, around 0.001% of the band gap values themselves, which are on the order of 1 eV, indicating that the iFFT method has captured the phonon-driven evolution of the band gap and is capable of an accurate prediction.

Figure 3 shows the ab initio and iFFT predicted NACs. NAC is the key parameter that governs nonradiative phonondriven charge trapping and recombination, which limit efficiencies of solar cells and other optoelectronic devices. The NAC has a more complex dependence on system geometry than the energy gap, and therefore, it is harder to predict. The iFFT and ab initio data show larger deviations for the NACs, Figure 3, than for the energy gaps, Figure 2. Nevertheless, the iFFT predictions based on the 1.56% data sampling are quite accurate. The mean square errors in the NAC are  $6 \times 10^{-5}$  meV for the band gap in pristine MAPbI<sub>3</sub>, 3  $\times$  10<sup>-5</sup> meV for the band gap in pristine CsPbI<sub>3</sub>, and 6  $\times$  10<sup>-6</sup>,  $2 \times 10^{-3}$ , and  $3 \times 10^{-5}$  meV for the trap-VBM, trap-CBM, and CBM-VBM transitions in defective CsPbI<sub>3</sub>. Since the absolute values of the NAC are on the order of 1-10 meV, the errors are still small, ranging from within 0.001-0.1%.

The NAC in MAPbI<sub>3</sub> exhibits notable fast fluctuations that are not captured by the 64 fs iFFT sampling, Figure 3a. The high-frequency fluctuations are more prominent in the NAC than in the energy gap, Figure 2a. Sampling the low frequencies allows us to reproduce only the longer scale fluctuations, and it remains to be seen whether such sampling is sufficient to achieve accurate NAMD time scales. Note that by filtering out higher frequencies, the iFFT interpolation underestimates heights of many peaks; however, at the same time, it also underestimates minima in the absolute NAC values. As a result, the average absolute NAC values are reproduced well, although the root-mean-square (RMS) NAC are slightly underestimated, Table 1.

The NAC can become very large and even diverge to infinity, when the two levels become degenerate. A moderate example of such a situation occurs in the CBM-trap NAC in defective CsPbI<sub>3</sub> at the early time in the middle panel of Figure 3c. The NAC increases 10-fold relative to its other values along the trajectory. At the same time, the corresponding energy gap becomes very small, middle panel of Figure 2c. The sampled data capture this fluctuation, while the iFFT interpolation slightly overestimates the fluctuation magnitude. In comparison, a NN with a comparable amount of training data underestimated somewhat the fluctuation magnitude, <sup>30</sup> while a

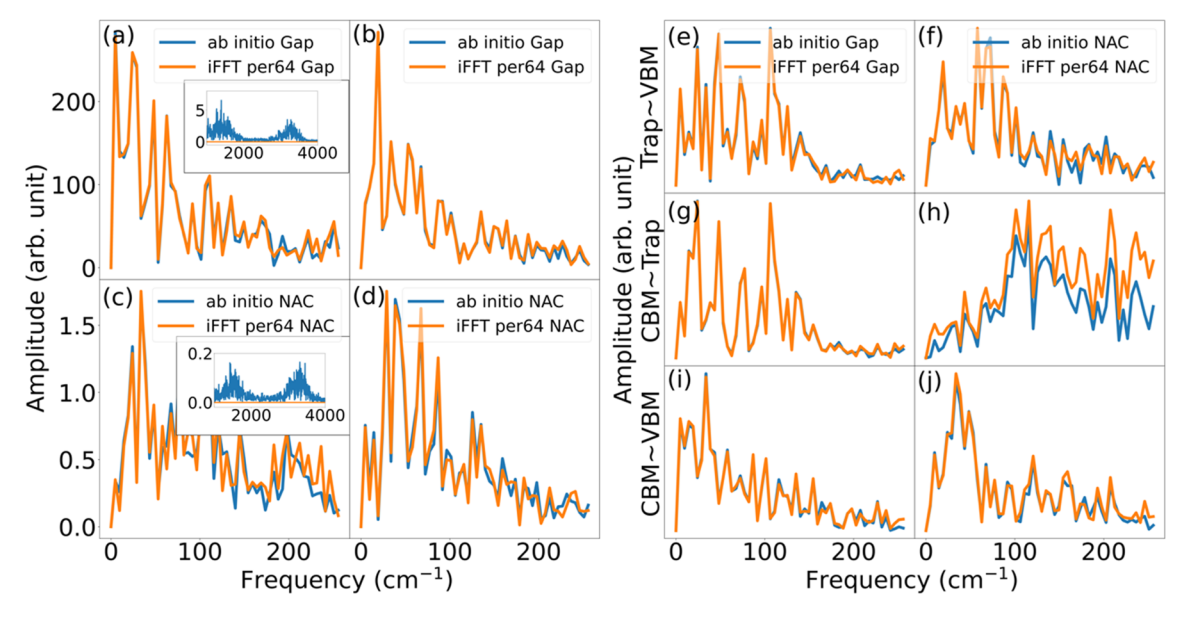


Figure 4. FTs of gap and NAC of (a, c) pristine MAPbI<sub>3</sub>, (b, d) pristine CsPbI<sub>3</sub>, and (e-j) defective CsPbI<sub>3</sub>, corresponding to the data shown in Figures 2 and 3. Every 64 points from the ab initio data are sampled to obtain the iFFT results. The iFFT method properly samples the most important, low-frequency modes. High-frequency vibrations of the MA species, shown in the insets of panels a and c, are not captured. However, the amplitude of the signals is small, and missing the MA motions has little influence on the NAMD results, Figure 5a.

KRR model reproduced this peak accurately using twice more training data. <sup>32</sup> One expects that low sampling should underestimate peak amplitudes, which is the case for other NAC peaks in Figure 3. The unusual behavior of the iFFT prediction of the large fluctuation in the CBM—trap NAC at the early time requires further investigation. For example, the results obtained for the very low sampling frequency, once every 256 fs, show that if a large peak is present and is sampled, then nearby NAC values are overestimated, since the interpolated data decay more slowly than the ab initio NAC, which exhibits a sharp fluctuation, Figure S4. Large NAC fluctuations represent important NAMD events. In particular, the large fluctuation governs the electron trapping process.

It is interesting to note that iFFT interpolation assumes that the data passed are continuous, and therefore, the end of the trajectory smoothly matches the beginning. This is a useful feature when NAMD Hamiltonians are iterated under the CPA. Iteration of a raw ab initio Hamiltonian creates a discontinuity, and the discontinuity is smoothed out by the iFFT interpolation.

The frequency analysis is presented in Figure 4, which shows FTs of the evolutions of the ab initio and iFFT energy gaps and NACs. The iFFT results reproduce the ab initio spectra well. The spectra are heavily dominated by low-frequency motions. This is a general phenomenon in nanoscale and condensed matter systems. 44–48 Changes in system geometries arising from local displacements of atoms with respect to each other, giving rise to high-frequency modes, tend to average out and have little overall influence on the energy and NAC. On the other hand, longer scale motions, such as radial breathing modes in carbon nanotubes, 46,49 breathing modes in nanocrystals, 50,51 and out-of-plane undulations of 2D systems 45,52 have strong influence on energy gaps and NACs. According to eq 1, the frequency of the NAC oscillation is determined by the frequency of the nuclear modes that induce changes in the electronic wave functions. In the current system, the wave functions are localized on the heavy Pb and I atoms, and the dominant frequencies arise from slow motions of these atoms.

Motions of the light atoms of the MA species have only an indirect influence on the electronic properties. The inserts in Figure 4a,c demonstrate two broad high-frequency peaks in the ab initio data, arising from stretching and bending of the N–H, C–H, and C–N bonds. These signals are missing entirely from the iFFT signals. However, the high-frequency signals are weaker by an order of magnitude for the NAC and by nearly 2 orders of magnitude for the gap, compared to the low-frequency signals, and therefore, high-frequency contributions to the energy gap and NAC should have little influence on the NAMD simulation results.

The NAMD simulation results obtained with the ab initio and iFFT Hamiltonians are presented in Figure 5, which shows rise or decay of populations of the key states during the electron—hole recombination dynamics. In pristine MAPbI<sub>3</sub>

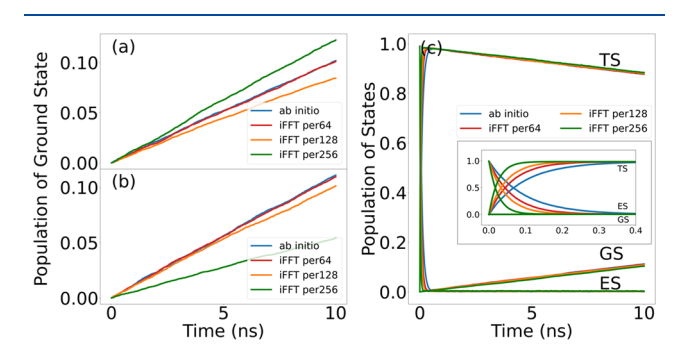


Figure 5. NAMD results showing populations of ground state (GS), excited state (ES), and trap state (TS) during the electron—hole recombination dynamics of (a) pristine MAPbI $_3$ , (b) pristine CsPbI $_3$ , and (c) defective CsPbI $_3$ . Along with the main iFFT results obtained by sampling every 64 data points, shown are the results based on sampling every 128 points (0.781% of data, 54 points in total) and 256 points (0.391% of data, 27 points in total). Insert in panel c presents detailed dynamics between TS and ES. Sampling only ~1% of ab initio data provides good estimates of the trapping and recombination times, Table 1.

and CsPbI<sub>3</sub> the ground-state population increases from 0 to 0.1 in 10 ns, which indicates a 10% probability that the electron recombines with the hole. In addition to the iFFT results obtained on the basis of sampling 1.56% of the ab initio data (every 64 fs), shown are the iFFT-NAMD results obtained with 0.781% (every 128 fs) and 0.391% (every 256 fs) of the data. Remarkably, sampling only 4 geometries per 1 ps already gives a correct order of magnitude estimate of the charge carrier lifetime in the pristine systems, while it matches the ab initio estimate of the carrier recombination in defective CsPbI<sub>3</sub> nearly perfectly, Figure 5c. Charge trapping occurs faster in the iFFT-NAMD calculations than in the ab initio NAMD, insert in Figure 5c. This is because iFFT overestimates the large fluctuation in the NAC at the beginning of the trajectory, middle panel of Figure 3c, as also reflected in the overestimated amplitudes of the FT signals shown in Figure 4h. The instance when the CBM-trap NAC is unusually large, and the corresponding energy gap is small, middle panel of Figure 2c, represents an approach to a conical interaction and dominates the charge trapping process. Importantly, the iFFT results converge systematically to the ab initio results as the sampling is increased. All-in-all, the iFFT-NAMD method allows one to obtain valuable estimates of charge trapping and recombination times in the MHPs with only ~1% of the ab

Tables 1 and S1 summarize canonically averaged energy gaps, absolute NACs, RMS NACs, pure-dephasing times, and NAMD transition times. The pure-dephasing times reported in the tables are obtained from the energy gap fluctuations using the second-order cumulant approximation to of the optical response theory.<sup>53</sup> The pure-dephasing time is used as the decoherence time of the DISH algorithm. 42 In most cases, the pure-dephasing times become slightly shorter with reduced data sampling, indicating that fluctuation of the energy gap is slightly overestimated, since the pure-dephasing times decrease with increasing gap fluctuation.<sup>53</sup> The NAMD transition times are computed by fitting the population data to appropriate exponential functions or their short-time linear approximations, such as  $P(t) = \exp(-t/\tau) \approx 1 - t/\tau$ . The electron–hole recombination times in the pristine systems obtained with iFFT-NAMD converge to within 1% of the ab initio NAMD results at the 1.56% sampling. They correlate with the accuracy of the NAC. According to the perturbative Fermi golden rule expression, the transition time depends on the coupling squared.<sup>54</sup> The charge trapping time (CBM-trap, Table S1) converges to the ab initio result as well; however, it remains too short because the iFFT method overestimates the NAC fluctuation event that governs the trapping: see the early time of the trajectory in the middle panel of Figure 3c. While the 1.56% sampling allows for an accurate description of both the energy gaps and the NAC, Figures 2 and 3, further sampling reduction causes substantial errors, Figures S1-S4. However, it is quite remarkable that a very low sampling frequency, once every 256 fs, gives reasonable estimates of the charge trapping and recombination time scales, even though the iFFT interpolation can predict only rough features of the time dependence of the ab initio NAMD Hamiltonian, Figures S2 and S4. This observation ties with the stochastic Hamiltonian method of Akimov.<sup>55</sup> Overall, the 1.56% iFFT-NAMD model shows an excellent agreement with the corresponding ab initio calculations, providing a very simple strategy to reduce the NAMD cost by nearly 2 orders of magnitude.

Charge trapping across relatively large energy gaps and charge recombination across the band gap are very important processes in optoelectronic applications, and they constitute an important application of the method. The iFFT-NAMD method can allow one to increase the system size in studying fast processes involving charge relaxation and separation through dense manifolds of conduction and valence band states. Modeling of processes driven by spin—orbit and Coulomb couplings, such as intersystem crossings and Auger-type phenomena, <sup>56,57</sup> can also be accelerated by iFFT-NAMD. Typically, the spin—orbit and Coulomb couplings fluctuate slower than the NAC, since they do not contain an explicit dependence on the nuclear velocity. Therefore, the iFFT-NAMD method can provide even larger computational savings.

In summary, we have developed an iFFT-NAMD method that can considerably reduce the computational cost of ab initio NAMD. The method is simpler than ML models and requires even less data sampling. Because NAMD in nanoscale materials is often governed by low-frequency long-scale acoustic-type motions, which have a stronger influence on the electronic properties than high-frequency local optical modes, it is sufficient to sample the ab initio NAMD Hamiltonian once every several tens or even hundreds of femtoseconds, providing a significant computational saving. The strategy of interpolating the NAMD Hamiltonian along a precomputed trajectory is much more efficient than the efforts aimed at predicting the NAMD Hamiltonian forward in time; however, it requires the CPA or similar assumption. In order to achieve a high overall NAMD efficiency while maintaining the ab initio level of description, the iFFT-NAMD method can be combined with MLFFs, which are now routinely generated and available for many materials and molecules. The method has been demonstrated with several MHPs that exhibit complex nuclear and electronic dynamics occurring on multiple time scales; are among the most widely studied materials; combine features of inorganic, organic, and even liquid matter; and provide an excellent testing ground of NAMD methodologies. The iFFT-NAMD method can provide computational savings in most cases, and the extent of the efficiency increase depends on the system and process under investigation. The current ab initio NAMD simulations of nanoscale systems are limited to a few or tens of picoseconds, and tens or a few hundred atoms. The developed strategy paves the way for extending the simulations to hundreds of picoseconds or nanoseconds, and/ or to many hundreds or thousands of atoms.

#### ASSOCIATED CONTENT

#### **Solution** Supporting Information

The Supporting Information is available free of charge at https://pubs.acs.org/doi/10.1021/acs.jpclett.1c03884.

Energy gaps and nonadiabatic couplings predicted with reduced data sampling (PDF)

#### AUTHOR INFORMATION

#### **Corresponding Author**

Oleg V. Prezhdo — Department of Chemical Engineering and Department of Chemistry, University of Southern California, Los Angeles, California 90089, United States; orcid.org/0000-0002-5140-7500; Email: prezhdo@usc.edu

#### Authors

Bipeng Wang — Department of Chemical Engineering, University of Southern California, Los Angeles, California 90089, United States; orcid.org/0000-0003-0924-5867 Weibin Chu — Department of Chemistry, University of Southern California, Los Angeles, California 90089, United States; orcid.org/0000-0001-5951-0337

Complete contact information is available at: https://pubs.acs.org/10.1021/acs.jpclett.1c03884

#### **Notes**

The authors declare no competing financial interest.

#### ACKNOWLEDGMENTS

The work was supported by the U.S. National Science Foundation, Grant No. CHE-1900510.

#### REFERENCES

- (1) Nottoli, M.; Cupellini, L.; Lipparini, F.; Granucci, G.; Mennucci, B. Multiscale Models for Light-Driven Processes. *Annu. Rev. Phys. Chem.* **2021**, 72, 489–513.
- (2) Smith, B.; Akimov, A. V. Modeling Nonadiabatic Dynamics in Condensed Matter Materials: Some Recent Advances and Applications. *J. Phys.: Condens. Matter* **2020**, 32, 073001.
- (3) Zheng, Q. J.; Chu, W. B.; Zhao, C. Y.; Zhang, L. L.; Guo, H. L.; Wang, Y. N.; Jiang, X.; Zhao, J. Ab Initio Nonadiabatic Molecular Dynamics Investigations on the Excited Carriers in Condensed Matter Systems. WIREs Comput. Mol. Sci. 2019, 9, e1411.
- (4) Crespo-Otero, R.; Barbatti, M. Recent Advances and Perspectives on Nonadiabatic Mixed Quantum-Classical Dynamics. *Chem. Rev.* **2018**, *118*, 7026–7068.
- (5) Mai, S. B.; Gonzalez, L. Molecular Photochemistry: Recent Developments in Theory. *Angew. Chem., Int. Ed.* **2020**, *59*, 16832–16846.
- (6) You, P. W.; Chen, D. Q.; Lian, C.; Zhang, C.; Meng, S. First-Principles Dynamics of Photoexcited Molecules and Materials Towards a Quantum Description. *WIREs Comput. Mol. Sci.* **2021**, 11, e1492.
- (7) Wang, L. J.; Akimov, A.; Prezhdo, O. V. Recent Progress in Surface Hopping: 2011–2015. *J. Phys. Chem. Lett.* **2016**, *7*, 2100–2112.
- (8) Prezhdo, O. V. Modeling Non-Adiabatic Dynamics in Nanoscale and Condensed Matter Systems. *Acc. Chem. Res.* **2021**, *54*, 4239–4249.
- (9) Akimov, A. V.; Prezhdo, O. V. The Pyxaid Program for Non-Adiabatic Molecular Dynamics in Condensed Matter Systems. *J. Chem. Theory Comput.* **2013**, *9*, 4959–4972.
- (10) Akimov, A. V.; Prezhdo, O. V. Advanced Capabilities of the Pyxaid Program: Integration Schemes, Decoherenc:E Effects, Multiexcitonic States, and Field-Matter Interaction. *J. Chem. Theory Comput.* **2014**, *10*, 789–804.
- (11) Shi, R.; Fang, W. H.; Vasenko, A. S.; Long, R.; Prezhdo, O. V. Efficient Passivation of Dy Center in CH3NH3PbBr3 by Chlorine: Quantum Molecular Dynamics. *Nano Res.* **2021**, *14*, DOI: 10.1007/s12274-021-3840-y
- (12) Qiao, L.; Fang, W. H.; Long, R.; Prezhdo, O. V. Elimination of Charge Recombination Centers in Metal Halide Perovskites by Strain. *J. Am. Chem. Soc.* **2021**, *143*, 9982–9990.
- (13) Sarkar, R.; Kar, M.; Habib, M.; Zhou, G. Q.; Frauenheim, T.; Sarkar, P.; Pal, S.; Prezhdo, O. V. Common Defects Accelerate Charge Separation and Reduce Recombination in Cnt/Molecule Composites: Atomistic Quantum Dynamics. *J. Am. Chem. Soc.* **2021**, *143*, 6649–6656.
- (14) Doltsinis, N. L.; Marx, D. Nonadiabatic Car-Parrinello Molecular Dynamics. *Phys. Rev. Lett.* **2002**, *88*, 166402.
- (15) Chu, W. B.; Zheng, Q. J.; Prezhdo, O. V.; Zhao, J. Co2 Photoreduction on Metal Oxide Surface Is Driven by Transient

- Capture of Hot Electrons: Ab Initio Quantum Dynamics Simulation. J. Am. Chem. Soc. 2020, 142, 3214–3221.
- (16) Zhang, L. L.; Chu, W. B.; Zhao, C. Y.; Zheng, Q. J.; Prezhdo, O. V.; Zhao, J. Dynamics of Photoexcited Small Polarons in Transition-Metal Oxides. *J. Phys. Chem. Lett.* **2021**, *12*, 2191–2198.
- (17) Unke, O. T.; Chmiela, S.; Sauceda, H. E.; Gastegger, M.; Poltavsky, I.; Schütt, K. T.; Tkatchenko, A.; Müller, K.-R. Machine Learning Force Fields. *Chem. Rev.* **2021**, *121*, 10142–10186.
- (18) Kulichenko, M.; Smith, J. S.; Nebgen, B.; Li, Y. W.; Fedik, N.; Boldyrev, A. I.; Lubbers, N.; Barros, K.; Tretiak, S. The Rise of Neural Networks for Materials and Chemical Dynamics. *J. Phys. Chem. Lett.* **2021**, *12*, 6227–6243.
- (19) Poltavsky, I.; Tkatchenko, A. Machine Learning Force Fields: Recent Advances and Remaining Challenges. *J. Phys. Chem. Lett.* **2021**, *12*, 6551–6564.
- (20) Rogers, D.; Hahn, M. Extended-Connectivity Fingerprints. *Journal of Chemical Information Modeling* **2010**, *50*, 742–754.
- (21) Bartók, A. P.; Kondor, R.; Csányi, G. On Representing Chemical Environments. *Phys. Rev. B* **2013**, *87*, 184115.
- (22) Behler, J.; Parrinello, M. Generalized Neural-Network Representation of High-Dimensional Potential-Energy Surfaces. *Phys. Rev. Lett.* **2007**, *98*, 146401.
- (23) Smith, J. S.; Isayev, O.; Roitberg, A. E. Ani-1: An Extensible Neural Network Potential with Dft Accuracy at Force Field Computational Cost. *Chemical Science* **2017**, *8*, 3192–3203.
- (24) Bai, X.; Guo, X.; Wang, L. J. Machine Learning Approach to Calculate Electronic Couplings between Quasi-Diabatic Molecular Orbitals: The Case of DNA. *J. Phys. Chem. Lett.* **2021**, *12*, 10457—10464
- (25) Fu, T. R.; Frommer, K.; Nuckolls, C.; Venkataraman, L. Single-Molecule Junction Formation in Break-Junction Measurements. *J. Phys. Chem. Lett.* **2021**, *12*, 10802–10807.
- (26) King, D. S.; Truhlar, D. G.; Gagliardi, L. Machine-Learned Energy Functionals for Multiconfigurational Wave Functions. *J. Phys. Chem. Lett.* **2021**, *12*, 7761–7767.
- (27) Srivastava, M.; Howard, J. M.; Gong, T.; Rebello Sousa Dias, M.; Leite, M. S. Machine Learning Roadmap for Perovskite Photovoltaics. *J. Phys. Chem. Lett.* **2021**, *12*, 7866–7877.
- (28) Taylor, M. G.; Nandy, A.; Lu, C. C.; Kulik, H. J. Deciphering Cryptic Behavior in Bimetallic Transition-Metal Complexes with Machine Learning. *J. Phys. Chem. Lett.* **2021**, *12*, 9812–9820.
- (29) Zhou, G. Q.; Chu, W. B.; Prezhdo, O. V. Structural Deformation Controls Charge Losses in Mapbi(3): Unsupervised Machine Learning of Nonadiabatic Molecular Dynamics. *Acs Energy Letters* **2020**, *5*, 1930–1938.
- (30) Wang, B. P.; Chu, W. B.; Tkatchenko, A.; Prezhdo, O. V. Interpolating Nonadiabatic Molecular Dynamics Hamiltonian with Artificial Neural Networks. *J. Phys. Chem. Lett.* **2021**, *12*, 6070–6077.
- (31) Chu, W. B.; Saidi, W. A.; Prezhdo, O. V. Long-Lived Hot Electron in a Metallic Particle for Plasmonics and Catalysis: Ab Initio Nonadiabatic Molecular Dynamics with Machine Learning. *ACS Nano* **2020**, *14*, 10608–10615.
- (32) Wu, Y. F.; Prezhdo, N.; Chu, W. B. Increasing Efficiency of Nonadiabatic Molecular Dynamics by Hamiltonian Interpolation with Kernel Ridge Regression. *J. Phys. Chem. A* **2021**, *125*, 9191–9200.
- (33) Li, W.; She, Y. L.; Vasenko, A. S.; Prezhdo, O. V. Ab Initio Nonadiabatic Molecular Dynamics of Charge Carriers in Metal Halide Perovskites. *Nanoscale* **2021**, *13*, 10239–10265.
- (34) Bisquert, J. Unique Curve for the Radiative Photovoltage Deficit Caused by the Urbach Tail. J. Phys. Chem. Lett. **2021**, 12, 7840–7845.
- (35) Wang, X. J.; Li, T. S.; Xing, B. Y.; Faizan, M.; Biswas, K.; Zhang, L. J. Metal Halide Semiconductors Beyond Lead-Based Perovskites for Promising Optoelectronic Applications. *J. Phys. Chem. Lett.* **2021**, 12, 10532–10550.
- (36) Wu, Y. F.; Chu, W. B.; Vasenko, A. S.; Prezhdo, O. V. Common Defects Accelerate Charge Carrier Recombination in Cssni3 without Creating Mid-Gap States. *J. Phys. Chem. Lett.* **2021**, *12*, 8699–8705.

- (37) Juarez-Perez, E. J.; Haro, M. Perovskite Solar Cells Take a Step Forward. *Science* **2020**, *368*, 1309–1309.
- (38) Best Research-Cell Efficiency Chart. NREL: 2021.
- (39) Kresse, G.; Hafner, J. Ab Initio Molecular Dynamics for Liquid Metals. *Phys. Rev. B* **1993**, *47*, 558–561.
- (40) Perdew, J. P.; Burke, K.; Ernzerhof, M. Generalized Gradient Approximation Made Simple. *Phys. Rev. Lett.* **1996**, 77, 3865–3868.
- (41) Virtanen, P.; Gommers, R.; Oliphant, T. E.; Haberland, M.; Reddy, T.; Cournapeau, D.; Burovski, E.; Peterson, P.; Weckesser, W.; Bright, J.; et al. SciPy 1.0: Fundamental Algorithms for Scientific Computing in Python. *Nat. Methods* **2020**, *17*, 261–272.
- (42) Jaeger, H. M.; Fischer, S.; Prezhdo, O. V. Decoherence-Induced Surface Hopping. *J. Chem. Phys.* **2012**, *137*, 22A545.
- (43) Mangan, S. M.; Zhou, G. Q.; Chu, W. B.; Prezhdo, O. V. Dependence between Structural and Electronic Properties of Cspbi3: Unsupervised Machine Learning of Nonadiabatic Molecular Dynamics. *J. Phys. Chem. Lett.* **2021**, *12*, 8672–8678.
- (44) Chu, W. B.; Zheng, Q. J.; Prezhdo, O. V.; Zhao, J.; Saidi, W. A. Low-Frequency Lattice Phonons in Halide Perovskites Explain High Defect Tolerance toward Electron-Hole Recombination. *Science Advances* **2020**, *6*, eaaw7453.
- (45) Li, L. Q.; Long, R.; Bertolini, T.; Prezhdo, O. V. Sulfur Adatom and Vacancy Accelerate Charge Recombination in Mos2 but by Different Mechanisms: Time-Domain Ab Initio Analysis. *Nano Lett.* **2017**, *17*, 7962–7967.
- (46) Long, R.; Prezhdo, O. V. Asymmetry in the Electron and Hole Transfer at a Polymer-Carbon Nanotube Heterojunction. *Nano Lett.* **2014**, *14*, 3335–3341.
- (47) Stier, W.; Duncan, W. R.; Prezhdo, O. V. Thermally Assisted Sub-10 fs Electron Transfer in Dye-Sensitized Nanocrystalline TiO2 Solar Cells. *Adv. Mater.* **2004**, *16*, 240–244.
- (48) Liu, J.; Kilina, S. V.; Tretiak, S.; Prezhdo, O. V. Ligands Slow Down Pure-Dephasing in Semiconductor Quantum Dots. *ACS Nano* **2015**, *9*, 9106–9116.
- (49) Zhou, G. Q.; Cen, C.; Wang, S. Y.; Deng, M. S.; Prezhdo, O. V. Electron-Phonon Scattering Is Much Weaker in Carbon Nanotubes Than in Graphene Nanoribbons. *J. Phys. Chem. Lett.* **2019**, *10*, 7179–7187.
- (50) Kamisaka, H.; Kilina, S. V.; Yamashita, K.; Prezhdo, O. V. Ultrafast Vibrationally-Induced Dephasing of Electronic Excitations in Pbse Quantum Dot. *Nano Lett.* **2006**, *6*, 2295–2300.
- (51) Kilina, S. V.; Kilin, D. S.; Prezhdo, V. V.; Prezhdo, O. V. Theoretical Study of Electron-Phonon Relaxation in Pbse and Cdse Quantum Dots: Evidence for Phonon Memory. *J. Phys. Chem. C* **2011**, *115*, 21641–21651.
- (52) Wang, Z. L.; Altmann, P.; Gadermaier, C.; Yang, Y. T.; Li, W.; Ghirardini, L.; Trovatello, C.; Finazzi, M.; Duo, L.; Celebrano, M.; et al. Phonon-Mediated Interlayer Charge Separation and Recombination in a Mose2/Wse2 Heterostructure. *Nano Lett.* **2021**, 21, 2165–2173.
- (53) Akimov, A. V.; Prezhdo, O. V. Persistent Electronic Coherence Despite Rapid Loss of Electron-Nuclear Correlation. *J. Phys. Chem. Lett.* **2013**, *4*, 3857–3864.
- (54) Hyeon-Deuk, K.; Madrid, A. B.; Prezhdo, O. V. Symmetric Band Structures and Asymmetric Ultrafast Electron and Hole Relaxations in Silicon and Germanium Quantum Dots: Time-Domain Ab Initio Simulation. *Dalton Transactions* **2009**, 10069–10077.
- (55) Akimov, A. V. Stochastic and Quasi-Stochastic Hamiltonians for Long-Time Nonadiabatic Molecular Dynamics. *J. Phys. Chem. Lett.* **2017**, *8*, 5190–5195.
- (56) Zhou, G. Q.; Lu, G.; Prezhdo, O. V. Modeling Auger Processes with Nonadiabatic Molecular Dynamics. *Nano Lett.* **2021**, *21*, 756–761.
- (57) Habenicht, B. F.; Prezhdo, O. V. Ab Initio Time-Domain Study of the Triplet State in a Semiconducting Carbon Nanotube: Intersystem Crossing, Phosphorescence Time, and Line Width. *J. Am. Chem. Soc.* **2012**, *134*, 15648–15651.

### ☐ Recommended by ACS

#### Increasing Efficiency of Nonadiabatic Molecular Dynamics by Hamiltonian Interpolation with Kernel Ridge Regression

Yifan Wu, Weibin Chu, et al.

OCTOBER 12, 2021

THE JOURNAL OF PHYSICAL CHEMISTRY A

READ 🗹

## Adiabatic Molecular Orbital Tracking in Ab Initio Molecular Dynamics

Asylbek A. Zhanserkeev, Ryan P. Steele, et al.

JULY 29, 2021

JOURNAL OF CHEMICAL THEORY AND COMPUTATION

READ 🗹

#### Nonadiabatic Molecular Dynamics on Graphics Processing Units: Performance and Application to Rotary Molecular Motors

Laurens D. M. Peters, Christian Ochsenfeld, et al.

NOVEMBER 25, 2019

JOURNAL OF CHEMICAL THEORY AND COMPUTATION

READ 🗹

#### Accelerating Realtime TDDFT with Block-Orthogonalized Manby-Miller Embedding Theory

Kevin J. Koh, John Parkhill, et al.

JULY 19, 2017

JOURNAL OF CHEMICAL THEORY AND COMPUTATION

READ 🗹

Get More Suggestions >